the response of the earth to deformations at tidal, annual, and Chandler periods is different from that at seismic periods. The effect of anelasticity is to make Chandler periods 1 to 2 days longer than the periods calculated for earth models constructed on the basis of short-period seismic data.

DON L. ANDERSON
HIROO KANAMORI
ROBERT S. HART
HSI-PING LIU

Seismological Laboratory, California Institute of Technology, Pasadena 91125

References and Notes

1. W. Futterman, *J. Geophys. Res.* **67**, 5279 (1962); E. Strick, *Geophys. J. R. Astron. Soc.* **13**, 197 (1967); C. Lomnitz, *J. Appl. Phys.* **28**, 201 (1957); H. Kolsky, *Philos. Mag.* **8**, 693 (1956).
2. H. Jeffreys, *Nature (London)* **208**, 675 (1965).
3. E. Carpenter and D. Davies, *ibid.* **212**, 134 (1966).
4. M. Randall, *Phys. Earth Planet. Inter.* **12**, 1 (1976).
5. H. Liu, D. Anderson, H. Kanamori, *Geophys. J. R. Astron. Soc.* **47**, 41 (1976).
6. D. Anderson, *ibid.* **14**, 135 (1967); J. Vaisnys, *J. Geophys. Res.* **73**, 7675 (1968); D. Jackson, *Proc. Natl. Acad. Sci. U.S.A.* **68**, 1577 (1971).
7. J. Savage, *J. Geophys. Res.* **70**, 3935 (1965).
8. C. Zener, *Elasticity and Anelasticity of Metals* (Univ. of Chicago Press, Chicago, 1948); S. Kogan, *Izv. Acad. Sci. USSR Earth Phys.* **11**, 3 (1966).
9. A. S. Norwick and B. S. Berry, *IBM J. Res. Dev.* **5**, 297 (1961).
10. R. Gordon and C. Nelson, *Rev. Geophys.* **4**, 457 (1966); D. Jackson, *Geophys. J. R. Astron. Soc.* **25**, 25 (1971).
11. D. Anderson and R. Kovach, *Proc. Natl. Acad. Sci. U.S.A.* **51**, 168 (1964); S. Smith, *Tectonophysics* **13**, 601 (1972).
12. D. Anderson, A. Ben-Menahem, C. Archambeau, *J. Geophys. Res.* **70**, 1441 (1965).
13. T. Jordan and D. Anderson, *Geophys. J. R. Astron. Soc.* **36**, 411 (1974); F. Gilbert and A. Dzienwonski, *Philos. Trans. R. Soc. London Ser. A* **278**, 187 (1975).
14. D. Anderson and R. Hart, *J. Geophys. Res.* **81**, 1461 (1976).
15. R. O'Connell and B. Budiansky, *ibid.* **79**, 5412 (1974).
16. D. Anderson, *Bull. Seismol. Soc. Am.* **54**, 681 (1964).
17. ———, *ibid.*, p. 681; ——— and R. Kovach, *ibid.* **59**, 1667 (1969), R. Wiggins, *Phys. Earth Planet. Inter.* **1**, 20 (1968).
18. T. Jordan, *Nature (London)* **257**, 745 (1975).
19. H. Jeffreys and K. Bullen, *Seismological Tables* (British Association for the Advancement of Science, London, 1940).
20. We are indebted to Sir Harold Jeffreys, who has consistently maintained that free oscillation and body wave data could not be compared directly because of the importance of damping. The role of damping has also been recognized by D. Davies, E. Carpenter, C. Lomnitz, and M. J. Randall. We wish to particularly thank M. J. Randall, who pointed out to us the inadequacy of current treatments of attenuation. This research was supported by the Advanced Research Projects Agency of the Department of Defense and was monitored by the Air Force Office of Scientific Research under contract F44620-77-C-0022. Contribution No. 2740, Division of Geological and Planetary Sciences, California Institute of Technology.

16 August 1976; revised 7 December 1976

Nuclear Morphometry During the Cell Cycle

Abstract. *Directly measured and derived geometric and densitometric parameters were obtained by means of the automated image analyzer Quantimet 720-D in Feulgen-stained HeLa cells synchronized by selective mitotic detachment. These data indicate substantial alteration of nuclear morphology during the entire cell cycle, even during the G1 and G2 phases, and the late G1–early S and late S–G2 transitions.*

Recent chemical and physicochemical studies of chromatin isolated from bulk populations of synchronized cells suggest that chromatin conformation (*1, 2*) and levels of nuclear protein phosphorylation (*3*) change throughout the mammalian cell cycle, parallel to other physical-chemical and autoradiographic parameters (*4*). Attempts have been made to correlate these variations with the mechanisms that control cellular proliferation and S phase DNA replication (*2, 3*). It is, however, difficult to estimate the degree to which measurement artifacts are introduced in these determinations by the physical alterations of macromolecular structure which are produced during the process of fractionation of cell constituents. For instance, there is evidence that the structural and functional properties of native chromatin are drastically altered by shearing during the isolation procedure (*5, 6*). It is desirable to determine quantitative changes in chromatin during the cell cycle in situ, that is, in cells that are morphologically intact. The DNA content of Feulgen-stained cell nuclei and chromosomes may be estimated by means of the integrated optical density (I.O.D.) obtained by scanning densitometers (*7*). Measurement artifacts usually arise from random processes such as variation in nuclear thickness and electrical noise in the measurement system, thus making statistical analysis necessary. These studies determined that differences in mean values of nuclear geometric parameters and I.O.D. (DNA content) exist between images obtained from cells that were synchronized and harvested at various intervals throughout the HeLa S3 cell cycle.

Several alternative approaches to texture analysis have already been used successfully in various fields of life science (*8*).

We measured the following parameters for each nuclear image at the base threshold [0.04 optical density (O.D.)]: I.O.D., area, projection, and perimeter. We also computed these derived parameters from measured values—average O.D. for each nuclear image (obtained by dividing the area of the nuclear image by the square of its parameter) and mean bounded path (obtained by dividing the area of a nuclear image by its horizontal projection). In this case the horizontal projection consisted of the linear sum of all lagging edges projected against a vertical line.

We used the Quantimet 720-D automated image analyzer for these experiments, which was equipped with a plumbicon scanner and 720-D densitometer module (Cambridge Instrument) (*9*), and a Reichert Zetopan research microscope, equipped with an 80-μm stage driven by a stepping motor. A 100-watt tungsten halogen light source was used, equipped with a 546-nm filter (40-nm bandwidth; Fish-Sherman). The condenser aperture was 1.35; the objective was 100 × oil immersion planar achromat with open iris and a numerical aperture of 1.25. Internal magnification was 10 ×, produced by a Reichert high-quality, direct coupled magnification changer.

The area scanned by the Quantimet is comprised of 880 by 688 picture points which are subdivided into a 32 by 24 shade correction matrix. A featureless area of the specimen is imaged and loaded into the shade corrector matrix. This provides a multipoint image loading of shading with omnidirectional interpolation throughout and across matrix squares. During specimen analysis, the video signal is routed through the shade corrector that modulates the signal to provide on-line background smoothing. The shade corrector compensates for local gray level differences in the image and provides a flat background field throughout the scanned region. The linear dimension of the square picture points was determined at the magnification used by means of a stage micrometer (American Optical) graduated in 20-μm divisions. The frame was adjusted to include leading and trailing edges at a given distance, and the frame width in picture points was read from the display (repeated ten times and averaged). The resultant mean picture point width (0.089 μm) was then entered into the data acquisition program and formed the basis for all measurements of length and area. Final system performance was checked by measuring the I.O.D. and area of a single nucleus (Fig. 1), which was manually positioned at seven different locations within the scanning field—one in the center of the field, one in each corner, and two on the center line (at the top

and the bottom of the field). The coefficients of variation of these parameters represent estimations of the effects of both nonuniformity and random electrical noise during the time required to make the individual measurements (about 5 minutes). The coefficients of variation were 2.4 percent for I.O.D. and 1.0 percent for area. Variation of both parameters was less than 0.5 percent for ten measurements of a single nuclear image in the center of the field.

Logarithmically growing HeLa S3 cells were maintained in suspension culture in Joklik-modified Eagle's minimum essential spinner medium (*10*) supplemented with 3.5 percent each of calf serum and fetal calf serum. Synchronization of cells (*11, 12*) was carried out in a warm room at 37°C for 18 hours. During this period, smears were prepared from the same culture at 1, 3, 5, 8, 12, 15, and 18 hours after selective detachment. The smears for each postdetachment time were hydrolyzed with 1*N* HCl for 15 minutes and stained with Schiff reagent for 60 minutes according to the method of DeCosse and Aiello (*13*); after staining, the samples were mounted in Canada balsam. These studies were made to determine whether differences in measured or computed geometric and densitometric parameters could be inferred to exist within cell cycle phases and across cell cycle phase boundaries (see Table 1). The following tests were performed for any parameter measured at the several points throughout the cycle.

1) Bartlett's test for homogeneity of variance (*14*). Because variance increases during the cycle as the cells became progressively desynchronized (*1*), this test always yielded a significant result.

2) A Welch test of equality of means that does not require an assumption of homogeneity of variance (*15*) (see Table 1).

3) Two-tailed Student's *t*-tests (*14–16*), not involving assumptions of homogeneity of variance, were used to compare the mean of a parameter with the mean values of the same parameter observed at the next earliest and next latest postdetachment times. The significance level for each comparison was 2.5 percent. These tests were employed to determine whether a given parameter changed within a cycle phase or across a phase boundary.

The degree of cell synchrony achieved by selective mitotic detachment is high and consistent with previous results (*1*), as seen by the time course of I.O.D. after mitosis. Figure 2 shows that mean DNA content (I.O.D.) of Feulgen-stained HeLa cells remains constant from 3 to 8 hours, increasing through 12 (middle-late S) to 15 hours (G2), decreasing again to the I.O.D. value of G1 (3 to 5 hours) at 18 hours after mitosis. These results are in agreement with the labeling and mitotic indices of HeLa cells pulse labeled with [^{3}H]thymidine (*1*), which indicates that DNA synthesis begins at 7 to 8 hours, reaching its peak at 12 hours, and falls to low levels at 18 hours after mitotic selection. The same data (*1*) showed quite a few mitoses at 1 to 2 hours after selective detachment, which is consistent with a slightly higher mean I.O.D. at 1 than at 3 hours.

On the other hand, geometric parameters such as area and perimeter (Fig. 2, lower panel) and projection (Fig. 3, upper panel) show modulation of chromatin morphology during the cell cycle that is not necessarily correlated with DNA content. Each mean value for a given time after mitosis was statistically tested, as previously described, against its previous and subsequent val-

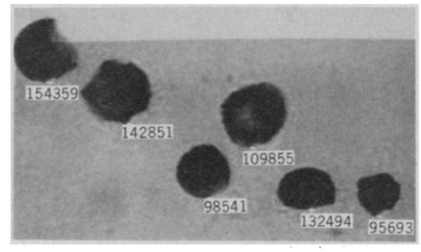

Fig. 1. Nuclear images of Feulgen-stained HeLa cells whose borders are defined by optical density (O.D.) of 0.04. The number beneath each cell indicates the I.O.D. value of the cell. Optical density was calibrated as follows: 100 percent transmission (0.0 O.D.) was defined by a clear area of the slide (accomplished by setting the controls so that 250,000 of the total of 500,000 picture points were indicated). The densitometer was then calibrated for infinite O.D. by blanking all light to the scanner. A 1.0 O.D. density filter was then inserted into the light path (using the same clear area of the slide) and the densitometer was adjusted, by means of calibration controls, until a threshold setting 1.0 on the densitometer resulted (again using the 250,000 picture point criterion). This procedure produced an overall linear calibration from 0.0 to 2.0 O.D. [Because the light transfer characteristic of the plumbicon is linear (0.99), the threshold calibration was linear throughout the operating range of the plumbicon tube.] All geometric parameters were computed within the borders defined by 0.04 O.D.

Table 1. Measured and computed mean parameter values observed in samples of synchronized HeLa cells as the population progressed through the cell cycle. Time represents the hours after selective detachment. Welch tests of each data set indicated that significant differences existed between individual means. The minimum sample size was 96 and the maximum 105. Numbers in parentheses represent the bounds of 1 standard deviation. Abbreviation: A.U., arbitrary unit.

Time (hours)	Parameter						
	I.O.D. (A.U. × 10^4)	Average O.D. (A.U. × 10^3)	Area (μm^2)	Projection (μm)	Perimeter (μm)	Form factor (no dimension) × 10^{-2}	Mean bounded path (μm)
01	11.6 (8.5–14.7)	1.51 (1.22–1.81)	77.7 (56.8–98.5)	11.3 (9.0–13.6)	38.2 (30.8–45.6)	5.32 (4.3–6.6)	6.74 (5.7–8.0)
03	10.0 (8.02–12.0)	1.631 (1.37–1.94)	61.74 (49.2–74.3)	9.52 (8.4–10.7)	31.7 (27.4–35.9)	6.13 (5.4–6.9)	6.4 (5.6–7.3)
05	10.6 (7.8–13.4)	1.81 (1.48–2.21)	60.79 (40.6–81.0)	9.90 (7.9–11.9)	32.1 (24.8–39.4)	5.9 (4.8–7.3)	5.99 (5.0–7.2)
08	9.45 (7.49–11.4)	1.87 (1.52–2.3)	52.22 (36.7–67.7)	10.4 (7.7–13.1)	33.8 (24.6–42.9)	4.61 (3.2–6.7)	4.97 (4.2–5.9)
12	13.4 (9.4–17.4)	1.70 (1.34–2.16)	76.63 (59.0–94.3)	14.4 (9.6–19.2)	45.4 (31.8–59.1)	3.86 (2.4–6.2)	5.41 (4.1–7.2)
15	14.8 (10.9–18.7)	1.92 (1.56–2.36)	77.3 (56.5–98.1)	11.3 (9.4–13.1)	36.2 (29.3–43.2)	5.92 (4.8–7.3)	6.76 (5.6–8.2)
18	10.2 (8.1–12.3)	1.68 (1.35–2.08)	61.18 (43.6–78.8)	10.11 (7.0–13.2)	32.8 22.2–43.5)	5.97 (4.4–8.0)	5.93 (4.9–7.2)

ues. Differences in chromatin area can be found between late G1 and early S, even though DNA content remains practically constant. Computation of derived parameters, such as average optical density (average O.D.) (Fig. 2, upper panel), mean bounded path, and form factor (Fig. 3), shows that chromatin morphology does change significantly at 1 hour (early G1), 3 hours (mid-G1), and 5 hours (late G1). Steadily increasing average O.D. and a parallel decrease in mean bounded path during this interval indicate a condensation of chromatin that is not detectable by any other means (*1–4*). Furthermore, between 5 hours (late G1) and 8 hours (early S) both form factor and mean bounded path abruptly decrease, while the I.O.D. is not significantly altered. Between 8 and 12 hours (mid-late S), the form factor decreases substantially and the mean bounded path increases slightly (but significantly). In the interval between 12 and 15 hours (late S–G2 transition), average O.D., mean bounded path, and form factor increase sharply (indicating a condensation of chromatin and a change in the nuclear border toward more circular geometry). On the other hand, it seems that chromatin dispersion increases (decrease in average O.D.) from early S to middle-late S, decreasing to the original late G1–early S value when the cells reach G2 (15 hours). These variations in average O.D., paralleling the abrupt variation in form factor (indicating a modulation of shape), are in perfect agreement with previous findings on isolated chromatin conformation as detected by circular dichroism and ethidium bromide binding sites (*1*) during the HeLa cell cycle. The agreement is striking between the time course of the changes of primary binding sites (*1*) and changes in chromatin dispersion and convolution as indicated by the average O.D., mean bounded path, and form factor, in the 3- to 15-hour interval. Furthermore, while form factor (Fig. 2) is indistinguishable between G2 (15 hours) and G1 cells (3, 5, and 18 hours), the decrease of mean bounded path (Fig. 2) is accompanied by a large decrease in average O.D. (Fig. 1), which is compatible with increasing chromatin dispersion as the cells from G2 return to G1.

These geometric and densitometric data from synchronized Feulgen-stained HeLa cells are interesting for two reasons. (i) They confirm, in chromatin observed in situ [see also (*17*)] the same results observed in "isolated" chromatin by independent physical-chemical techniques, indicating substantial alterations in chromatin conformation during the cell cycle (*4*). (ii) They prove to be quite powerful with respect to the characterization of chromatin morphology with a high degree of accuracy, even during the G1 phase (traditionally indicated as a "gap" or "black box," but now capable of subdivision into objectively identifiable subcompartments, with the same DNA content but different geometric properties). Also, this method could allow characterization of chromatin morphology during the late G1–early S transition (where most antimetabolites act and variations in DNA content are minimal) and between the G2 and G1 phases. These studies, conducted on Feulgen-stained, synchronized HeLa cells, prove that geometric and densitometric texture analyses may constitute a unique tool for achieving a newer understanding of the biology of cell growth and kinetics. Their impact on life science is promising, mostly because of the possibility of extending such analyses to sections of intact tissues (*18*).

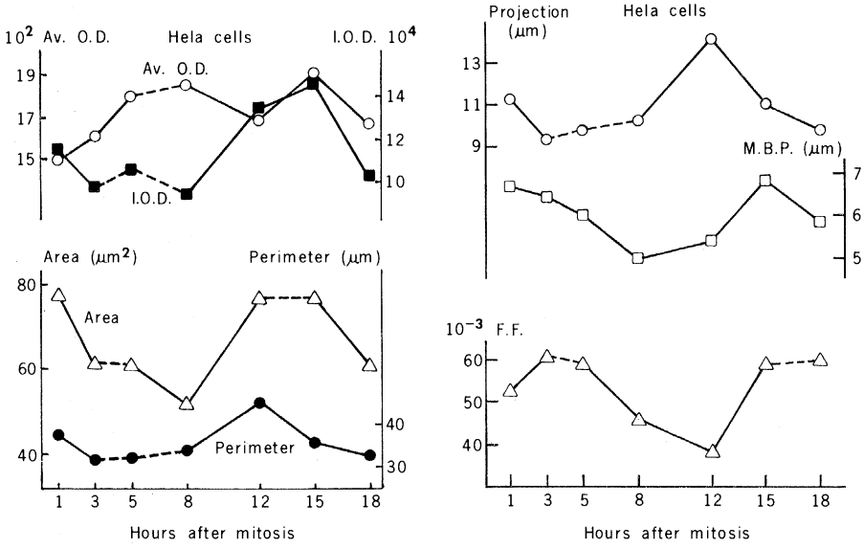

Fig. 2 (left). Mean integrated optical density (*I.O.D.*), area, perimeter, and average optical density (*Av. O.D.*) (obtained by dividing the I.O.D. by the area) for each nuclear image of synchronized HeLa S3 cells at various time intervals after mitosis. The data acquisition program was set to ensure that at least 100 nuclear images would be analyzed on any given slide. Acquisition was subject to the visual control of an operator who provided a "go" or "no go" command. If a given field contained overlapping nuclear images or staining artifacts it was skipped, and the microscope stage was moved in 80-μm steps until another promising field appeared. The acquired data of all thresholds were spooled onto casettes as ASCII text files, and subsequently transferred to a disk. Three computer programs were written to permit screening and extraction of raw values for specific parameters and subsequent statistical testing of the means and variances that resulted (*16*). The dashed lines mean that adjacent values were not significant at the 2.5 percent level, while solid lines connecting two mean values indicate that the differences between such means were significant at the 5 percent level. Fig. 3 (right). Mean values of projection, form factor (*F.F.*), and mean bounded path (*M.B.P.*) of Feulgen-stained HeLa cells, at various intervals after mitotic selective detachment. Data at the higher thresholds included area, projection, and perimeter, but only the base value data at threshold of 0.04 O.D. are reported. As noted in the legend to Fig. 2, dashed lines mean that adjacent values were *not* significant in two-tailed Student's *t*-tests at the 2.5 percent level, while solid lines connecting two means indicate a significant difference.

F. KENDALL
R. SWENSON
Division of Biophysics, Temple University Health Sciences Center, Philadelphia, Pennsylvania 19140
T. BORUN
J. ROWINSKI
Wistar Institute, Philadelphia, Pennsylvania
C. NICOLINI*
Division of Biophysics, Temple University Health Sciences Center

References and Notes

1. C. Nicolini, A. Kozu, T. Borun, R. Baserga, *J. Biol. Chem.* **250**, 3381 (1975).
2. R. Baserga and C. Nicolini, *Biophys. Biochim. Acta* **458**, 109 (1976).
3. D. Marks, W. Paik, T. Borun, *J. Biol. Chem.* **248**, 5560 (1973).
4. C. Nicolini, *J. Natl. Cancer Inst.* **55**, 821 (1975).
5. M. Noll, J. O. Thomas, R. D. Kornberg, *Science* **187**, 1203 (1975).
6. C. Nicolini, R. Baserga, F. Kendall, *ibid.* **192**, 796 (1976).
7. M. L. Mendolsohn, D. A. Hungerford, G. H. Mayall, B. Perry, T. Conway, J. M. S. Prewitt, *Ann. N.Y. Acad. Sci.* **157**, 376 (1969).
8. G. L. Wied, Ed., *Introduction to Quantitative Cytochemistry* (Academic Press, New York, 1966), vols. 1 and 2; J. Rowinski, W. Sawiki, R. Swenson, H. Koproski, *Acta Cytol.* **19**, 136 (1975); M. Bibbo, P. H. Bartels, G. F. Bobr, J. Taylor, G. L. Wied, *ibid.* **17**, 340 (1973); P. H. Bartels, G. B. Olson, J. Layton, R. Anderson, G. L. Wied, *ibid.* **16**, 53 (1972).
9. G. Fisher and C. P. Bond, *Microscope* **20**, 203 (1972).
10. D. F. Peterson, R. A. Tobey, E. L. Anderson, *Fed. Proc. Fed. Am. Soc. Exp. Biol.* **28**, 1771 (1969).
11. T. Terasima and L. J. Tolmach. *Exp. Cell Res.* **30**, 344 (1963).

12. E. Robbins and P. I. Marcus, *Science* **144**, 1152 (1964).
13. J. J. Decosse and N. Aiello, *J. Histochem. Cytochem.* **14**, 601 (1966).
14. W. J. Dixon and F. J. Massey, Jr., *Introduction to Statistical Analysis* (McGraw-Hill, New York, 1969), p. 308.
15. B. L. Welch, *Biometrika* **38**, 330 (1951).
16. F. M. Kendall, G. Loffredo, C. A. Nicolini, Internal Report 7/75 (Biophysics Division, Temple University Health Sciences Center, Philadelphia, 1975).
17. G. Moser, R. Muller, E. Robins, *Exp. Cell Res.* **91**, 73 (1975).
18. C. Nicolini, *Biophys. Biochim. Acta* **458**, 243 (1976).
19. Supported by National Cancer Institute grants CA-20034, CA-18258, CA-12923, and CA-11463. T.B. is a recipient of research career development award CA-00088.
* Send all correspondence and reprint requests to C.N.

22 November 1976

Direct Resorption of Bone by Human Monocytes

Abstract. *Cultured human peripheral blood monocytes stimulate the release of bone mineral and matrix from killed long bones of fetal rats. These effects were inhibited by cortisol but were not altered by hormones that normally stimulate osteoclastic bone resorption. There was no evidence of morphologic differentiation of the monocytes into osteoclasts during bone resorption.*

Monocytes and macrophages are often seen adjacent to bone-resorbing surfaces in patients with chronic inflammatory diseases, such as rheumatoid arthritis, periodontal disease, and cholesteatoma, and also in those with tumors that metastasize to bone. Monocytes and macrophages are also found in the normal bone-marrow cavity adjacent to remodeling endosteal bone surfaces. However, although there is in vivo experimental evidence that osteoclasts may be derived from circulating mononuclear cells (*1*), there has been no evidence that these cells themselves are capable of direct bone resorption. We have now shown that circulating human monocytes can stimulate bone mineral and matrix resorption in vitro.

Human peripheral blood monocytes were obtained from normal blood donors at the Connecticut Red Cross, Farmington, Connecticut. Human leukocytes were obtained from plateletpheresis donations from normal donors. After the platelets had been removed from the other blood cells in the plateletpheresis apparatus, red cells were separated by dextran sedimentation to leave a leukocyte buffy coat. The neutrophils in the leukocyte buffy coat were removed by Ficoll-Hypaque (Pharmacia) density sedimentation. When cells were suspended for 90 minutes in medium containing 20 percent fetal calf serum in plastic petri dishes at 37°C in an atmosphere of 5 percent CO_2 and air, monocytes adhered to the plastic surfaces (*2*). The nonadherent lymphocytes were removed by gently rinsing the plastic petri dishes with fresh, warmed medium. Macrophages were grown as colonies from human bone-marrow aspirates cultured on semisolid mediums (*3*) (McCoy's 5A in methylcellulose—4000 count sec^{-1}) (Fisher) with 10 percent fetal calf serum and 5 percent horse serum. Macrophage colonies were clearly discernible between the 10th and 12th days of culture. The nature of these colonies was confirmed by Wright's staining of smeared cells.

The assay for bone resorption used in these experiments has been described (*4*). Pregnant rats at the 18th day of gestation were subcutaneously injected with 0.2 mc of ^{45}Ca or 1 mc of [^{3}H]proline. The next day, the fetal rat radius, ulna, and tibia were removed, and the mineralized shafts were dissected free from the cartilaginous ends and adjacent soft tissue. The bones were killed by freeze-thawing three times and were then exposed to ultraviolet light for several hours. The bones were either split or left intact and were then cultured with the cell preparations for 5 to 8 days. The cells were cultured in BGJ medium (Gibco) supplemented with either bovine serum albumin (4 mg per milliliter of medium) or 10 percent fetal calf serum inactivated by heat. Bone resorption was measured as the release of ^{45}Ca from the cultured bones into the medium. Values were expressed as means ± standard errors for four pairs of bone cultures. Statistical differences were analyzed with *t*-tests. In some experiments the rat bones were labeled with [^{3}H]proline to measure matrix resorption, expressed as the percent of total radioactivity released into the medium during the period of culture (*5*).

Table 1. Bone mineral release in the presence of cultured human mononuclear cells from paired killed bones previously incorporated with ^{45}Ca. Cells were cultured for 5 days in BGJ medium supplemented with 4 mg of bovine serum albumin per milliliter of medium at a density of 1×10^6 cells per milliliter. Results are expressed as ratios of ^{45}Ca released from killed bones cultured with the indicated cells to that released from paired bones cultured without the cells. Values are means ± standard errors for four pairs of bone cultures.

Culture	Ratio (treated-to-control)
Mononuclear cells	1.37 ± .14*
Adherent mononuclear cells	1.30 ± .03*
Nonadherent mononuclear cells	1.13 ± .03*

*Significantly greater than 1.0 ($P < .05$, *t*-test).

When human mononuclear cells, from which neutrophils were separated by Ficoll-Hypaque sedimentation, were cultured with killed bones for 5 to 8 days, there was an increase in both ^{45}Ca release (Table 1) and [^{3}H]proline release from the bones compared with the comparison (paired) bones cultured without cells. When the cells were cultured for 8 days with four pairs of bones previously labeled with [^{3}H]proline, the treated-to-control ratios for radioactivity released into the medium were 1.52 ± 0.13 ($P < .01$; Table 1). The greatest increase in mineral release from the killed bones occurred between the 4th and the 8th days of culture (Table 2). The mononuclear cells were much more effective in resorbing killed bone than the nonadherent population ($P < .01$; Table 1).

Monocytes are not the only cells we have found to cause bone resorption directly. Fetal rat calvarial cells also cause matrix resorption and mineral release from dead bones, although their effects are usually much greater than those of monocytes (*6*). During an 8-day period, calvarial cells cause a 40 to 200 percent increase in mineral release compared with paired bones cultured without cells, whereas monocytes usually cause a 30 to 60 percent increase in mineral release. Marrow macrophages are also capable of resorbing killed bone. When colonies of macrophages obtained from normal human bone marrow aspirate were cultured on semisolid mediums, adjacent but noncontiguous killed long bones of fetal rats were visibly resorbed during a 48-hour period between the 10th and 12th days of culture. None of the other cells that have been tested under these conditions [including nonadherent human lymphocytes (Table 1), rat fibroblasts, and nonadherent rat spleen cells] have caused mineral to be released from killed bones.

Hormones that normally stimulate osteoclastic bone resorption and mineral release from live bones in organ culture —such as parathyroid hormone (PTH), osteoclast activating factor (OAF), 1_{α},25-dihydroxycholecalciferol [1_{α},25-$(OH)_2D$], and prostaglandins-E_2 (PGE_2) —did not increase mineral release from killed bones stimulated by mononuclear cells during an 8-day period (Table 2). In a separate experiment (experiment 2), salmon calcitonin (SCT) (100 milliunits per milliliter of medium) did not inhibit